MATERIALS SCIENCE

Programmable light-driven swimming actuators via wavelength signal switching

Kai Hou[1,2], Dongshi Guan[3,4], Hangyu Li[3,4], Yongqi Sun[1,5], Yue Long[1]*, Kai Song[1,2]*

Light-driven swimming actuators with different motion modes could lead to many previously unachievable applications. However, controllable navigation often requires focusing light precisely on certain positions of the actuator, which is unfavorable for accurate dynamical operation or in microscale applications. Here, we present a type of programmable swimming actuators that can execute wavelength-dependent multidirectional motions via the Marangoni effect. Several multi–degree of freedom swimming motions have been realized: Forward-and-backward and zigzag actuators can execute one-dimensional (1D) and 2D linear motion, respectively; bidirectional gear rotation as angular motion can be regulated to obtain tunable speeds; and the turning actuator as a "freighter" is able to turn left, right, and go straight for precise maze navigation. A mechanical measurement system is established to quantitatively measure the driving force of the motion directly. The accessible wavelength-selective strategy presented here can inspire further explorations of simple and practical light-driven materials and systems.

INTRODUCTION

Self-propelled swimming actuators in miniature scale (submillimeter to centimeter) that can execute various motion modes in response to external stimuli have affected the designs of bioinspired motions (*1*–*3*), autonomous movements (*4*, *5*), and collective behaviors (*6*) and have attracted many interests for their promising applications in energy conversion (*7*, *8*), targeted drug delivery (*9*), biomedical engineering (*10*), and environment (*11*). Diverse actuating systems controlled by various driving forces such as electric field (*12*, *13*), magnetic field (*1*, *14*), chemical matter (*15*–*17*), and light (*18*–*21*) have been developed for swimming locomotion. Among these, light, as a ubiquitous and versatile stimulus, is able to provide not only spatial and temporal control but also modulation of diverse parameters such as intensity, wavelength, and polarization (*22*, *23*). Various light-driven swimming have been reported previously, such as light-induced deformation (*2*, *18*, *20*, *24*, *25*), vapor/bubble (*7*, *26*, *27*), chemical Marangoni effect (*19*, *21*, *28*), and thermal Marangoni effect (*9*, *29*–*31*).

Since the simple unidirectional motion actuator in one dimension (1D) is at its infancy stage (*18*, *32*), many efforts have been made to endow the light-driven swimming actuators with multifunctional motion modes. For instance, directional navigation has the potential to push or transport things through complicated paths, and rotation as angular motion is favorable for continuous gear transmission or stirring in small scale. Thus, there is an urgent need to make the swimming motion directional and controllable for advanced manipulation manner. To fulfill this requirement, one general strategy is to focus light on a specific domain of the actuator, subsequently, to generate partial impetuses to control the direction of motions (*20*, *21*, *24*, *29*, *31*). However, this focusing strategy seems to be complicated and to experience difficulty in executing dynamic, long-term, and microscale tasks that request stable high-accuracy light tracking and focusing. In contrast, whole-area light irradiation as a simple and stable manipulation free of light positioning enables swimming actuators to perform programmed motion modes. However, one actuator is programmed to have only one degree of freedom (DOF) under the whole-area irradiation, such as unidirectional moving (*33*) and rotation (*30*, *31*). Therefore, it is a challenge to design a programmable swimming actuator to realize both simple whole-area light operation and multi-DOF motions.

Light of specific wavelength interacts more strongly with elements that have stronger absorption at the wavelength, resulting in wavelength-selective responses of different absorbers. The wavelength-selective property has been used in fields such as photochemical reaction (*34*), optofluidic control (*35*), selective release (*36*), and soft actuators (*37*–*45*). For actuating systems, wavelength-selective units with disparate absorption can be programmed into elaborate layout; thus, partial response modes can be realized by light irradiation with different wavelengths.

Here, a series of programmable wavelength-selective swimming actuators that can execute multiple directional motions manipulated by whole-area irradiation of lights with specific wavelength are presented in this work. Two commercial photothermal dyes with different absorption properties, Oil red O and Prussian blue, were doped into polydimethylsiloxane (PDMS) to fabricate two modular wavelength-selective photothermal units. Then, the swimming actuators were fabricated by cutting and attaching the photothermal units to passive biaxially oriented polypropylene (BOPP) tape substrates. Upon the whole-area irradiation of laser with specific wavelength, the two units gave out heat both collectively and differently, giving rise to an asymmetric thermal distribution in the actuator. As a result, local surface tension of the water around decreased with local temperature increase, producing a partial surface tension gradient, along which a partial impetus was generated according to the Marangoni effect (*30*, *32*) to propel the actuator to move directionally. To quantitatively characterize the driving force of the Marangoni effect–based motion, the phenomenological acceleration was analyzed and the theoretical force was calculated. In addition, an experimental system for direct mechanical measurement was established. Using

[1]Key Laboratory of Bio-inspired Materials and Interfacial Science, Technical Institute of Physics and Chemistry, Chinese Academy of Sciences, Beijing 100190, P. R. China. [2]School of Future Technology, University of Chinese Academy of Sciences, Beijing 100049, P. R. China. [3]The State Key Laboratory of Nonlinear Mechanics, Institute of Mechanics, Chinese Academy of Sciences, Beijing 100190, P. R. China. [4]School of Engineering Science, University of Chinese Academy of Sciences, Beijing 100049, P. R. China. [5]Institute of Chemical Materials, China Academy of Engineering Physics, Mianyang 621900, P. R. China.
*Corresponding author. Email: longyue@mail.ipc.ac.cn (Y.L.); songkai@mail.ipc.ac.cn (K.S.)

the wavelength-selective strategy that can achieve both simple manipulation and multiple DOF motion, several functional motion modes have been realized. We designed linear actuators for simple 1D forward-backward motion and 2D expanded zigzag motion as linear translation. A gear actuator can execute continuous clockwise/counterclockwise rotation as an angular motion mode, and the angular speed can be regulated by varying the light intensity. Further, a turning actuator that can execute integrated motions is manipulated to flexibly transport a cargo through a maze. The functional motion modes exhibit the application potential for swimming tasks of the actuators.

RESULTS

Fabrication and characterization of photothermal units and actuators

The approach to achieve wavelength-selective photothermal in this work relies on differential light absorption of two photothermal units. PDMS precursors doped with two commercial available dyes, Oil red O and Prussian blue, were spin-coated and cured at 80°C for 2 hours to fabricate the photothermal units, Oil red O–doped PDMS (OR-PDMS) and Prussian blue–PDMS (PB-PDMS) (Fig. 1A and Materials and Methods). Unless otherwise specified, PB-PDMS [4 weight % (wt %), with a thickness of 270 μm] and OR-PDMS (1 wt %, with a thickness of 300 μm) were used as typical photothermal units (fig. S1, A and B). The dye-PDMS units were cut into shapes and attached to commercial BOPP tapes (with a thickness of 35 μm; fig. S1C) in designed layouts for fabrication of the dye-PDMS/BOPP actuators (fig. S2). The BOPP tapes were used as structural substrates and served as passive parts for photothermal inhibition and subsidiary programming (details are provided in note S1).

As shown in the ultraviolet-visible (UV-vis) absorption spectrum, the two photothermal units presented distinctive light absorption peaks (Fig. 1B and fig. S1, D and E). The OR-PDMS has a stronger absorption at 532 nm (green vertical line) than that of PB-PDMS,

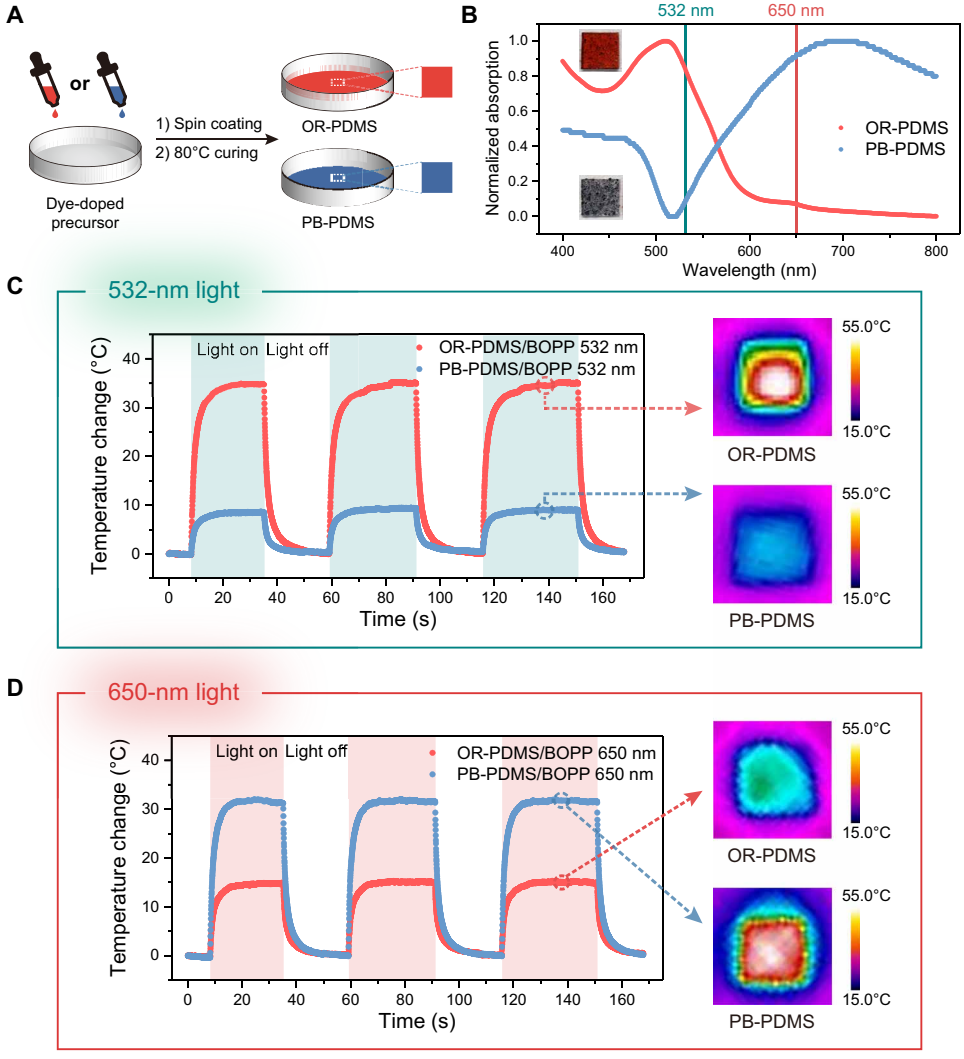

Fig. 1. Wavelength-selective photothermal units. (**A**) Schematic illustration of the fabrication procedure of dye-PDMS units. (**B**) Ultraviolet-visible (UV-vis) spectrum of the two dye-PDMS units shows selective absorption at wavelengths of 532 nm (green vertical line) and 650 nm (red vertical line). Insets are the optical images of OR-PDMS (top) and PB-PDMS (bottom). (**C** and **D**) Selective temperature changes of the dye-PDMS/BOPP on water surface upon 532-nm (C) and 650-nm (D) laser irradiation, respectively. Infrared (IR) images on the right present the selective photothermal properties of the units at their balanced temperature.

while the PB-PDMS has a stronger absorption at 650 nm (red vertical line) than that of OR-PDMS. Because of the different absorption properties, the units showed selective photothermal conversion abilities depending on the wavelength of the irradiated light (Fig. 1, C and D, and fig. S3). To investigate the wavelength-selective photothermal properties of the units, temperature changes and infrared (IR) images of the dye-PDMS/BOPP were measured statically on the water surface (initial water temperature of ca. 19° to 20°C) by a thermographic camera upon irradiation of 532- and 650-nm lasers (details are provided in Materials and Methods). Under the 532-nm laser (0.45 W cm^{-2}), the OR-PDMS obtained a larger temperature change of 35.0°C, while the temperature of PB-PDMS only increased 9.3°C (Fig. 1C). Under the 650-nm laser (1.6 W cm^{-2}), the OR-PDMS showed a larger temperature change of 31.8°C, while the temperature of PB-PDMS only increased 15.2°C (Fig. 1D). The results above demonstrate that the OR-PDMS/BOPP and PB-PDMS/BOPP gave out heat collectively but differently depending on specific wavelength. Further photothermal performances of the units were also studied by varying the light intensity (fig. S4) and dye content (fig. S5).

Mechanism: Swimming via the photothermal Marangoni effect

The mechanism of the dye-PDMS/BOPP actuator swimming on the water surface upon laser irradiation was studied (note S2, figs. S6 and S7, and movie S1). First, the motion behaviors of a pure PDMS/BOPP under 532-nm laser (1.6 W cm^{-2}) and 650-nm laser (1.6 W cm^{-2}), respectively, were examined. They displayed neither noticeable temperature rising nor substantial displacement. Then, we examined the motion behavior of an OR-PDMS/BOPP actuator under 532-nm laser (0.9 W cm^{-2}) on the pure water surface and that on the soaped water added with SDS surfactant. The actuator can swim repeatedly, driven by the 532-nm laser on the pure water, whereas, after adding the SDS surfactant into the water, the actuator stopped swimming under the same illuminating condition (fig. S6). These results suggest a swimming mechanism of the photothermal Marangoni effect (*9*, *29*–*31*). With the temperature of the water increasing around the photothermal region, the surface tension of the water decreases and leads to a surface tension gradient along which an impetus is generated to propel the actuator toward cooler region. The Marangoni effect is largely weakened by the low surface tension of the soaped water because of the existence of surfactant (*29*, *30*, *46*); for this reason, the OR-PDMS/BOPP cannot swim on the soaped water despite the accumulation of enormous heat (fig. S7, A to E, and movie S1).

The mechanism of deformation interaction can be excluded, as the propulsion force from device-water momentum exchange or energy storage is weakly influenced by the surface tension decrease (*18*), which is different from the Marangoni effect that is vulnerable to surface tension decrease (note S2 and fig. S6). In addition, dye-PDMS/BOPP/(larger-)BOPP actuators were also able to swim on the water surface but with a longer start-up time (the time from the beginning of irradiation to when obvious displacement is observed), demonstrating that chemical diffusion is not essentially involved in the process (note S2 and fig. S7, F and G).

Theoretical calculation and experimental characterization of the driving force

It is an important task to quantitatively estimate the driving force of the swimming motion driven by the photothermal Marangoni effect, by which one can verify the mechanism, make analysis/simulation, and search for further application scenarios. However, the estimation of the driving force relies on calculation of surface tension gradient or the analysis of phenomenological acceleration, lacking the support of mechanically experimental evidence. To quantitatively estimate the driving force of the light motion, we analyzed the phenomenological acceleration and calculated the theoretical force in the motions (note S3), and an experimental system was established for direct mechanical measurement (note S4 and movie S2).

Phenomenological acceleration analysis

Three light-driven motions of an actuator were recorded, and the displacement, velocity, and acceleration of the movements were analyzed (fig. S8). Because the acceleration is directly from the motion, it reflects the phenomenological force that represents the actual occurred force. According to Newton's second law, the maximum force calculated by the maximum acceleration is about 53 to 88 nN (table S1).

Theoretical calculation

We calculated the surface tension gradient and fluid resistance in the actuating processes at the time of maximum acceleration (note S2 and table S2). The surface tension of water is influenced by temperature as Harkins formula depicts (*31*)

$$\gamma = b_0 + b_1 T + b_2 T^2 \quad (1)$$

where γ is the surface tension, T is the temperature of the heated water (°C), b_0 = 75.796 mN m^{-1}, b_1 = −0.145 mN m^{-1} $°C^{-1}$, and b_2 = −0.00024 mN m^{-1} $°C^{-2}$. The temperature range of the heated water is obtained from the thermal images by color range selection (fig. S8). According to the symmetrical structural of the actuator, the circulation integral of the surface tension gradient can be simplified as

$$\oint_l \gamma \mathrm{d}l = (\gamma_0 - \gamma)\, l \quad (2)$$

where l is the length of contact margin between the photothermal unit and the heated water (3.2 mm; fig. S8). The surface tension difference between the front and rear of the actuator is calculated to be about 0.94 to 1.0 mN m^{-1}, and the gradient force is about 3.02 to 3.19 μN.

The fluid resistance f can be calculated as follows

$$f = \frac{1}{2} v^2 c \rho S \quad (3)$$

where ν is the motion velocity, ρ is the density of water, S is the contact area of the actuator-water interface, and c is the friction drag coefficient that is related to Reynolds number (Re) that can be calculated by $Re = vL/\mu$, where ν is the motion velocity, L is the characteristic length of the whole actuator (4 mm; fig. S8), and μ is the kinematic viscosity of water. The Re is calculated to be 22.9 to 33.8 (laminar flow state), so the c can be approximated as the friction drag coefficient for laminar flow ($c = 1.328\, Re^{-1/2}$) (*47*, *48*). The fluid resistance f is calculated to be 0.073 to 0.13 μN, which is in accordance with the magnitude of the maximum phenomenological resistance (0.071 to 0.093 μN).

Thus, the resultant driving force can be obtained by $F = \oint_l \gamma \mathrm{d}l - f$, and the result is about 2.95 to 3.06 μN (table S2).

Mechanical measurement

Although theoretical and phenomenological analysis have been used to estimate the driving force of actuators, to our best knowledge, direct mechanical measurement of the actuators on the water surface have not been conducted previously in the literature. Therefore, a glass needle-based mechanical system was developed to directly measure the driving force of the motion (Fig. 2, note S4, and movie S2). The glass needle with an end width of 3 μm was fabricated by a micropipette puller, and the tip of the glass needle was plunged into the water surface and was propelled by the light motion of an OR-PDMS/BOPP actuator (with a V-shape open for needle tip contact) upon 532-nm laser irradiation (0.8 W cm^{-2}). The maximum displacement of the needle Δx represents the maximum driving force of the actuator (Fig. 2, A to C, and table S3). Then, the glass needle was modified with a SiO_2 microsphere for liquid drop capture, and its stiffness was calibrated via added mass method that the force induced by the deformation of the needle that was mechanically calibrated by a series of mass known liquid drops (Fig. 2D, table S4, and fig. S9). Hence, the driving force is equivalent to the load gravity that causes the same needle deformation. According to the calibration curve that describes the relationship between load gravity (added mass) and the displacement of the glass needle (elastic deformation), the driving force of the light motion can be read to be about 61 to 109 nN (Fig. 2E).

The magnitude of the experimental value (0.061 to 0.109 μN) is closed to that of the phenomenological force (0.053 to 0.088 μN) but is smaller than that of the theoretical value (2.95 to 3.06 μN). The experimental measurement reduces the influence of complex dynamic during the movement; thus, the experimental value reflects the driving force more directly. These results indicate that (i) the driving force of the actuator in this system is about sub-hundred nanonewton (nN); (ii) the surface tension gradient does not fully contribute to the generation of impetus, which is probably due to the nonideal device-water contact line, space configuration of the concave water surface, or the thermocapillary convection beneath the water surface (note S4) (*46*).

Response regulation of the motion

The response property of the motion is important to regulate the performance of the swimming motion. In the swimming motion, the actuator would (i) move out of the light area in a few seconds and (ii) continue to swim by inertia until it stops. The speed of this process is difficult to regulate directly, but the response property of the swimming motions is more obviously influenced by the light intensity.

The response time (the time from the beginning of irradiation to when it reaches the maximum velocity) and the maximum velocity are chosen as two parameters to characterize the response property of the swimming motion. The response of the linear motions of two OR-PDMS/BOPP and PB-PDMS/BOPP actuators (4 mm by 4 mm; the same as those in figs. S6 to S8) was tested under two lasers with varying light intensities. The response time and maximum velocity were analyzed from the displacement time recordings.

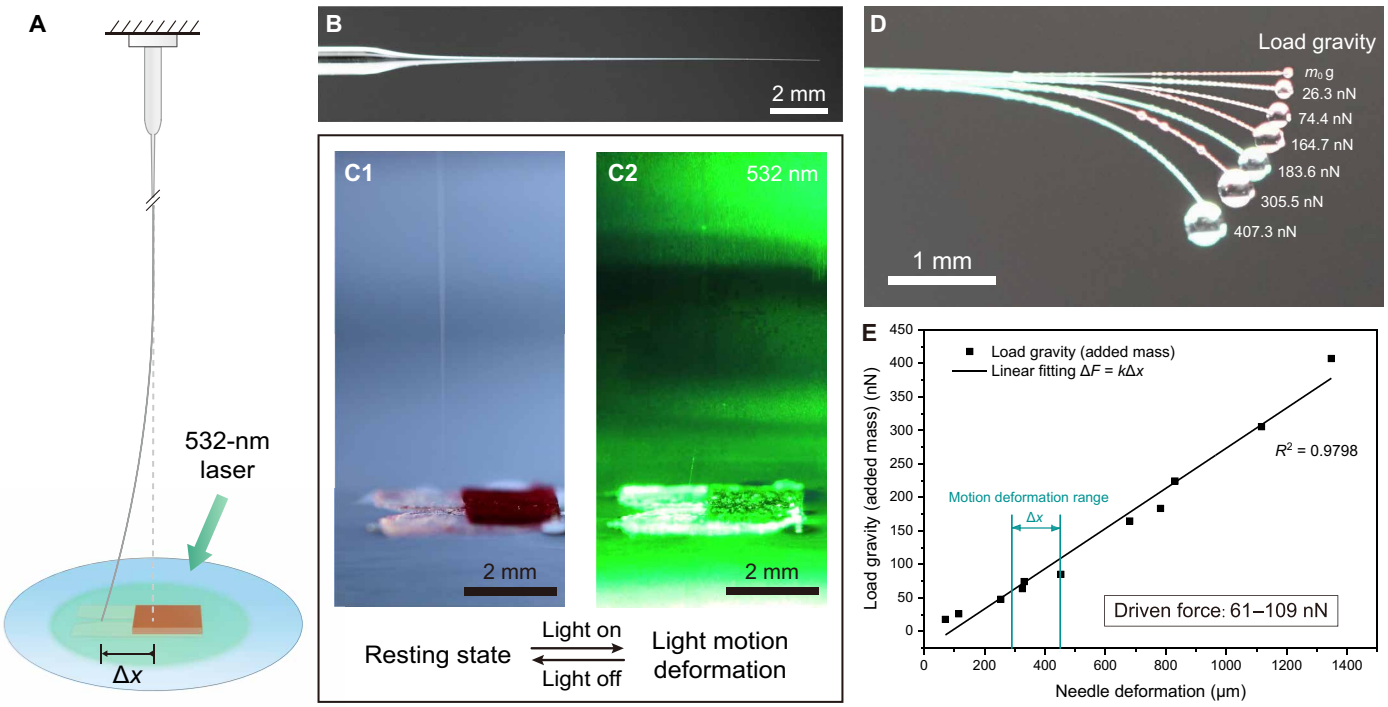

Fig. 2. Mechanical measurement. (**A**) Schematic of the light motion–induced elastic deformation of a glass needle. (**B**) The optical image of the glass needle for light motion measurement. (**C**) The resting state (C1) and the motion-induced elastic deformation upon 532-nm laser irradiation (C2) of the needle-actuator system. (**D**) The stiffness of the glass needle is calibrated by added mass method using a series of liquid drop (NOA81) with different gravities. The total gravity of each load is given, and m_0 is the original mass of the modified glass needle composed of cured UV adhesive and SiO_2 microsphere. (**E**) Calibration curve shows the relationship between load gravity (added mass) and needle deformation, and the driving force of the light motion can be inferred accordingly. Photo credit: Kai Hou, Technical Institute of Physics and Chemistry.

The relationship between the response time/maximum velocity and the light intensity was characterized; the results show that, in general, the higher intensity of the laser makes the motion occur faster and the maximum velocity of the motion higher. In addition, low-intensity light or weak photothermal effect (such as OR-PDMS/BOPP under 650-nm laser) might lead to unstable and irregular movement directions because of insufficient impetus.

Linear actuators

Linear motion as the basic mode of swimming represents the fundamental function for displacement. By programming the two photothermal units in para-position and orthogonal position, a forward-and-backward actuator and an L-shaped actuator were fabricated to perform bidirectional linear motion of forth-and-back motion and zigzag motion, respectively. The forward-and-backward actuator was composed of two rectangular dye-PDMS parts and a passive BOPP substrate with extended lateral sides for lateral photothermal inhibition (Fig. 3A). Upon 532- and 650-nm laser irradiation, OR-PDMS and PB-PDMS units in para-position gave out heat collectively but selectively, and the actuator displayed inverse thermal modes (Fig. 3B). The antagonistic photothermal between two sides results in a total surface tension gradient, along which a propulsion is induced via the Marangoni effect to propel the actuator toward the relatively cooler end in straight trajectory. Because the two thermal modes are wavelength dependent, the actuator can perform opposite bidirectional swimming and can be manipulated to execute a forth-and-back cruise task between two lights similar to a "ball" kicked by two "goalkeepers" (Fig. 3C; fig. S11, A and B; and movie S3). Between the green 532-nm laser (0.9 W cm^{-2}) and the red 650-nm laser (1.6 W cm^{-2}), the actuator swam toward the red region (1.10 cm s^{-1}) upon the 532-nm green light irradiation, and then the actuator swam backward (1.30 cm s^{-1}) toward the green region when it reached the 650-nm red light region.

On the basis of the 1D bidirectional motion, an L-shaped linear actuator is able to execute 2D in-plane linear motion by changing the intersection angle between the units. The L-shaped actuator was made by spacing two units perpendicularly like an "L" onto a BOPP substrate with extended lateral sides (Fig. 3D). Upon 532- and 650-nm laser irradiation, the L-shaped actuator displayed selective thermal modes at orthogonal directions (Fig. 3E); thus, the actuator can swim toward the direction that is perpendicular to the hotter long side driven by the Marangoni effect (fig. S11, C and D). The L-shaped actuator can perform orthogonally directional motions and can be manipulated to execute linear zigzag motion in response to alternative 532-nm (0.9 W cm^{-2}) and 650-nm (1.6 W cm^{-2}) lasers (Fig. 3F and movie S4). The linear actuator can be further programmed to vary the angle between motion vectors for potential applications such as autonomous tasks and execution of targeted paths.

Gear rotation actuator

Light-driven gear actuators that can rotate on the water surface have been demonstrated to have potential application for transmission and small-scale stirring. However, the torques of the rotation often originate from either precise partial/structural irradiation (*20*, *29*, *49*)

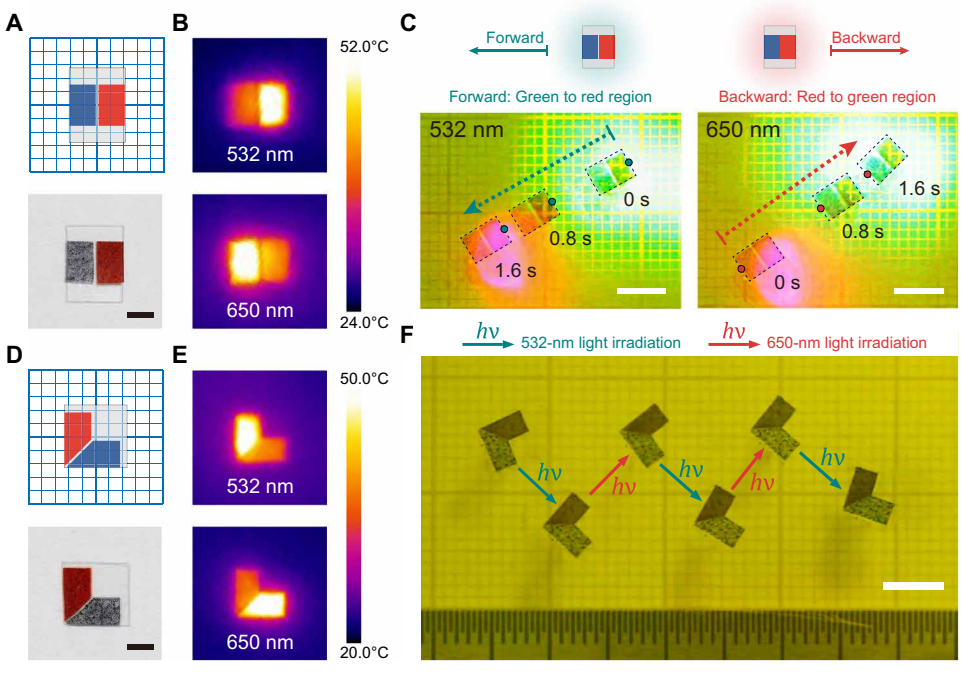

Fig. 3. Linear motion actuators. (**A**) Schematic illustration and optical image of the forward-and-backward actuator. Scale bar, 2 mm. (**B**) IR images show inverse thermal modes of the actuator on the water surface upon 532- and 650-nm laser irradiation, respectively. (**C**) Schematic illustration and superimposed photograph show the cruise motion of the forward-and-backward actuator between the green light region (532-nm laser) and the red light region (650-nm laser) (movie S3). The motion directions are instructed by arrows, and the units are outlined by dashed lines. Scale bars, 5 mm. (**D**) Schematic and optical image of the L-shaped actuator. Scale bar, 2 mm. (**E**) IR images show perpendicular thermal modes of the actuator under 532- and 650-nm laser on water, respectively. (**F**) Superimposed photograph shows the zigzag motion of the L-shaped actuator manipulated by alternative 532-nm laser (green arrow) and 650-nm laser (red arrow) (movie S4). Scale bar, 5 mm. Photo Credit: Kai Hou, Technical Institute of Physics and Chemistry.

or single DOF asymmetric structures (*10*, *30*, *31*). Here, we present a strategy to endow one gear actuator with clockwise- and counterclockwise-rotating directions, only being bound to specific wavelengths. Upon 532- or 650-nm laser irradiation, alternative OR-PDMS and PB-PDMS units in the gear presented alternative hotter/cooler thermal modes (Fig. 4, A and B). In each blade, the two units as counterparts have partial thermal distribution between the two sides, resulting in an impetus toward the cooler side via the Marangoni effect. In total, the forces on the four blades produced a total torque; thus, the gear actuator was propelled to rotate. When the motion reached a balance, the actuator rotated counterclockwise at an angular velocity of $\omega = 4.8$ rad s^{-1} under 532-nm laser (0.8 W cm^{-2}), while it rotated clockwise at $\omega = 3.7$ rad s^{-1} under 650-nm laser (1.6 W cm^{-2}) (Fig. 4C and movie S5). The sine value of the angular displacement ($\sin\theta$) as a function of time was calculated and was fitted using a sinusoidal curve, and the plots show that the gear rotates steadily upon continuous irradiation (Fig. 4D). Further, the angular velocity can be regulated by varying laser powers (Fig. 4, E and F). The gear actuator performs larger angular displacements being proportional to increased laser powers, and the angular velocity can be tuned from 2.7 to 7.6 rad s^{-1} and from 1.2 to 3.7 rad s^{-1} by shifting the intensities of 532- and 650-nm laser, respectively.

Turning actuator

Direction-controllable swimming navigation on the water surface, as the integrated motion mode that can navigate unlimitedly for targeted tasks, has applications for cargo transportation and biomedicine (*9*, *10*, *21*, *24*, *31*). Some attempts have been made to realize the direction-controllable swimming navigation; however, the navigations rely on precise light focusing on certain positions of the actuators. Although additional detection-and-tracking control systems can be used, it also seems difficult and unstable to navigate directionally in microscale or dynamic motion. Here, we demonstrate a turning actuator that is capable of left and right turn by wavelength signal switching instead of light position. Square OR-PDMS and PB-PDMS units were taped abreast on the BOPP substrate with reserved BOPP margin for front and lateral photothermal inhibitions (Fig. 5A and note S1). Under the laser irradiation, the asymmetric thermal distribution modes (Fig. 5B) lead to two tendencies: On one hand, because of the collective heat generation, the surface tension gradient between the dye-PDMS side (back) and the passive BOPP margin (front) produces a continuous tendency to move the actuator forward; on the other hand, the thermal selectivity between the left and right sides of the actuator results in unbalanced propulsion, leading to a torque that tends to rotate the actuator.

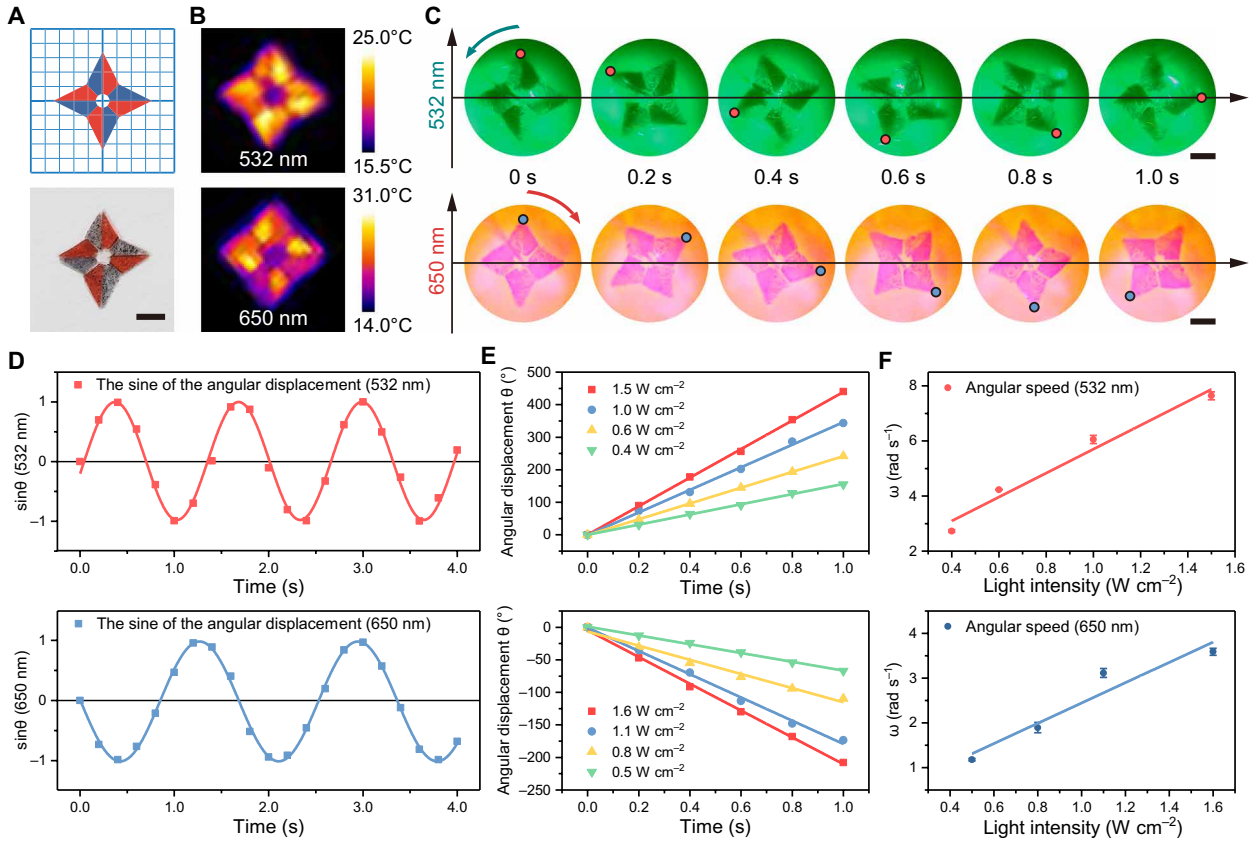

Fig. 4. Gear rotation actuators. (**A**) Schematic illustration and optical image of the gear actuator. (**B**) IR images show alternative thermal modes of the gear actuator upon 532- and 650-nm laser irradiation, respectively. (**C**) Sequencing images show that the gear actuator rotates counterclockwise and clockwise within 1 s upon 532-nm and 650-nm laser irradiation, respectively (movie S5). One end point of the gear actuator, which is marked by red/blue dots, shows the angular displacements of the rotation. (**D**) Sine of the angular displacement ($\sin\theta$) as a function of time and sine curve fitting show steady gear rotations under the lasers. (**E** and **F**) Angular displacement θ (E) and angular velocity ω (F) of the gear rotations can be regulated by varying laser powers. Scale bars, 2 mm. Photo Credit: Kai Hou, Technical Institute of Physics and Chemistry.

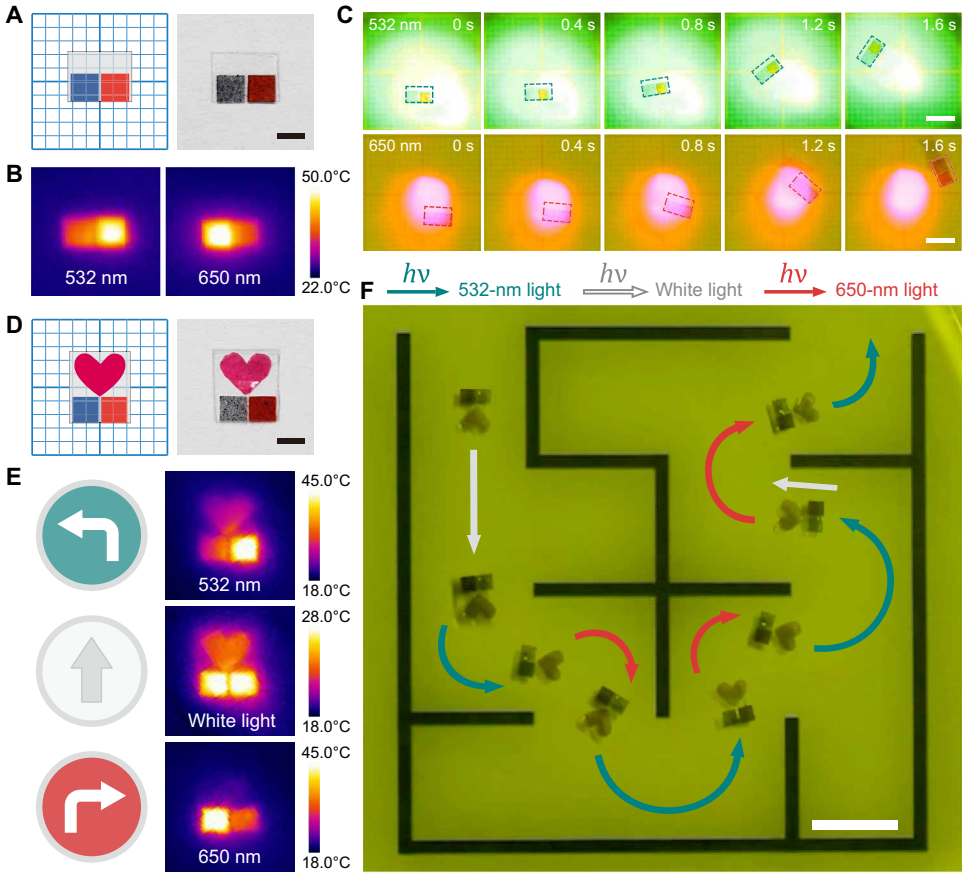

Fig. 5. Turning actuators and maze navigation. (**A**) Schematic illustration and optical image of the turning actuator. Scale bar, 2 mm. (**B**) IR images show the asymmetric thermal modes of the turning actuator on the water surface upon 532- and 650-nm laser irradiation, respectively. (**C**) Sequencing images of the left and right turning motions upon 532- and 650-nm laser irradiation, respectively (movie S6). The outlines of the actuator are marked by dashed lines. Scale bars, 5 mm. (**D**) Schematic and optical image of the "freighter" actuator loaded with a plastic heart cargo. Scale bar, 2 mm. (**E**) Directional signs and corresponding IR images of the actuator under 532-nm laser (top), compound white light (middle), and 650-nm laser (bottom). (**F**) Superimposed photograph shows that the freighter actuator can navigate through a maze manipulated by the three lights (movie S7). Scale bar, 2 cm. Photo credit: Kai Hou, Technical Institute of Physics and Chemistry.

The tendencies of forward moving and rotating indicate an arc trajectory of the turning motion (fig. S12). As the results show, when being irradiated by the 532-nm laser (0.9 W cm^{-2}) and 650-nm laser (1.6 W cm^{-2}), the actuator turned left-front and right-front in arc path, respectively (Fig. 5C; fig. S11, E and F; and movie S6). Besides, as a simpler model, when exposed to white light from a xenon lamp, the actuator moved straight forward because of similar photothermal effects of the two units upon white light irradiation (fig. S13).

A "freighter"-like turning actuator with a cargo was demonstrated to navigate through a maze manipulated by 532- and 650-nm laser and white light. The freighter actuator, loaded with a plastic heart (0.6 mg), had wavelength-dependent thermal modes, resulting in left/right/forward motion directions (Fig. 5, D and E). Manipulated by the three lights, the freighter actuator navigated through a maze (Fig. 5F and movie S7). This wavelength-selective strategy provides simple and stable control for the actuator to navigate in complex routes and execute further tasks such as pushing sliced objects on the water surface.

DISCUSSION

In summary, programmable light-driven swimming actuators that can execute multidirectional motions using wavelength-selective strategy was demonstrated in this work. Two wavelength-selective photothermal units contribute to specific asymmetric light-induced thermal modes of the dye-PDMS/BOPP actuators upon laser irradiation, along with partial impetuses via the Marangoni effect. Thus, the actuators can execute wavelength-selective multidirectional motions, including forward-and-backward (1D) and zigzag (2D) linear motions, and bidirectional gear rotation (angular motion), turning left and right and navigating through a maze (integrated motion mode). In this system, both simple manipulation and motions in multiple directions were taken into consideration. On one hand, the whole-area irradiation of single-wavelength light as a simple and stable manipulation is capable of precise dynamic light focusing. On the other hand, one actuator is endowed with multiple wavelength-dependent motion directions, each of which contributes one DOF. These designs make it feasible to realize effective dynamic operations, miniaturization of the systems, and execution of tasks with complex routes.

In this work, the driving force of the Marangoni effect–based light motion was estimated via theoretical calculation and phenomenological acceleration analysis, and an experimental system for mechanical measurement was proposed and established. This quantitative analysis and experimental measurement may provide evidence for solving mechanical problems, and this method is also available to be used for the mechanical measurement of small objects or insects on the water surface within nano- and micronewton range. In fabrication aspect, the materials used in this system are common, commercial, and low cost, and the fabrication method is facile and time saving. This accessibility provides possibility for large-scale manufacture, modular assembly or replacement, and customized programmable designs. It is expected that this work may provide a useful perspective toward the integration of programmable functions and inspire further explorations for advanced light-driven actuating systems using other parameters of light.

MATERIALS AND METHODS

Fabrication and characterization of the dye-doped PDMS units

The PDMS precursor was composed of a silicone base and a curing agent (10:1) (SYLGARD 184, Dow Corning) and was mixed with dyes, Oil red O (0.5 to 1 wt %; dye content of 70%; J&K, China) or Prussian blue (2 to 4 wt %; soluble, Sigma-Aldrich). The precursor mixture in petri dish was spin-coated by a spin coater (WS-650MZ-23NPPB, Laurell Technologies) and cured in an oven at 80°C for 2 hours. The prepared OR-PDMS and PB-PDMS units were cut into specific shapes by a razor for further assembly. The thickness of the dye-PDMS films was controlled by the spin speeds and was observed using a scanning electron microscope (SU-8010, Hitachi). The absorption properties of the dye-PDMS were measured using a UV-vis spectrophotometer (UV-2600, SHIMADZU).

Fabrication of the dye-PDMS/BOPP actuators

The two photothermal units were cut into different shapes and attached to a commercial BOPP tape substrate. The edges of BOPP were carefully cut by a razor blade to obtain desired BOPP margins of the dye-PDMS/BOPP actuators (details are provided in note S1 and fig. S1).

Photothermal measurements of the actuators

All the photothermal measurements were performed on the water surface to simulate the actuators during the motions (initial water temperature of ca. 19° to 20°C). Photothermal measurements of the dye-PDMS/BOPP were carried out upon light irradiation of an intensity-tunable 532-nm laser (NBT-532, Beijing NBET Technology, China), a 650-nm laser (equipped with a polarization filter externally for intensity tuning; Changchun Laser Optoelectronics Technology, China), and white light from a xenon lamp with an optical fiber (MAX 309, Beijing NBET Technology, China). The thermal information of the dye-PDMS/BOPP was recorded by a thermographic camera (A615, FLIR). A series of 3 mm by 3 mm square OR/PB-PDMS with different dye contents were attached to BOPP tapes and were used for photothermal property measurements. Each actuator was fixed by a cotton thread that floated under water in order to keep the actuator contacting the water surface, and the thermal distribution modes of the actuator upon light irradiation were recorded by the thermographic camera. Further photothermal properties were researched by varying the light intensity and dye contents (details are provided in figs. S4 and S5).

Mechanical measurement

The glass needle was fabricated by a micropipette puller equipment (P1000, Sutter Instrument Co.) with an end diameter of about 3 μm. The needle was held vertically to the water surface and controlled by a stepping motor (MC 1000e controller, Siskiyou, USA). A 4 mm by 4 mm OR-PDMS/BOPP actuator (with a V-shape open of the BOPP for needle locking) was used to propel the needle tip upon 532-nm laser irradiation (0.8 W cm^{-2}). The displacement of the needle tip was recorded by a digital camera (Canon EOS 90D with a macro lens) and analyzed by the snapshots of the videos (ImageJ) (details are provided in note S4).

Calibration of the glass needle

The force induced by the deformation of the needle was calibrated by a series of mass-known liquid drops. To capture the liquid drops to the tip of the needle, a SiO_2 microsphere (ϕ52 μm, Microspheres-Nanospheres, USA) was first glued to the needle tip with a small amount of UV curable glue (NOA81, Norland Products Inc., USA). The glue was cured under 365-nm UV light for 15 s (CS2010, Thorlabs, USA). Then, a series of viscous liquid drops (NOA81 glue) were transferred onto the SiO_2 microsphere by another glass needle for the calibration. The deflection of the needle and the size of the liquid drops were read using a stereomicroscope (MSV266, Leica, Germany) and a digital camera (Canon EOS 90D with a macro lens). The load gravity was calculated by the sum mass of [cured glue + SiO_2 + liquid drop–contained cylinder glass] (details are provided in note S4 and table S4).

Recording and analysis of the locomotion

Videos of the locomotion of the actuators were recorded using a camera (Canon EOS 80D with a macro lens) behind a 575-nm filter (NBT-575 nm, Beijing NBET Technology, China) for adapting to the high intensity of lasers. The thermal information during the motion was obtained by real-time recording using the thermographic camera. The tones of the snapshots of the videos were adjusted for obvious observation (details are provided in note S5).

SUPPLEMENTARY MATERIALS

Supplementary material for this article is available at https://science.org/doi/10.1126/sciadv.abh3051

View/request a protocol for this paper from *Bio-protocol*.

REFERENCES AND NOTES

1. Z. Ren, W. Hu, X. Dong, M. Sitti, Multi-functional soft-bodied jellyfish-like swimming. *Nat. Commun.* **10**, 2703 (2019).
2. S. J. Park, M. Gazzola, K. S. Park, S. Park, V. Di Santo, E. L. Blevins, J. U. Lind, P. H. Campbell, S. Dauth, A. K. Capulli, F. S. Pasqualini, S. Ahn, A. Cho, H. Yuan, B. M. Maoz, R. Vijaykumar, J. W. Choi, K. Deisseroth, G. V. Lauder, L. Mahadevan, K. K. Parker, Phototactic guidance of a tissue-engineered soft-robotic ray. *Science* **353**, 158–162 (2016).
3. L. Hines, K. Petersen, G. Z. Lum, M. Sitti, Soft actuators for small-scale robotics. *Adv. Mater.* **29**, 1603483 (2017).
4. C. A. Aubin, S. Choudhury, R. Jerch, L. A. Archer, J. H. Pikul, R. F. Shepherd, Electrolytic vascular systems for energy-dense robots. *Nature* **571**, 51–57 (2019).
5. R. F. Ismagilov, A. Schwartz, N. Bowden, G. M. Whitesides, Autonomous movement and self-assembly. *Angew. Chem. Int. Ed.* **41**, 652–654 (2002).
6. N. J. Suematsu, S. Nakata, A. Awazu, H. Nishimori, Collective behavior of inanimate boats. *Phys. Rev. E Stat. Nonlin. Soft Matter Phys.* **81**, 056210 (2010).
7. T. Luan, F. Meng, P. Tao, W. Shang, J. Wu, C. Song, T. Deng, Bubble-enabled underwater motion of a light-driven motor. *Small* **15**, e1804959 (2019).
8. X. Yang, M. Cheng, L. Zhang, S. Zhang, X. Liu, F. Shi, Electricity generation through light-responsive diving-surfacing locomotion of a functionally cooperating smart device. *Adv. Mater.* **30**, 1803125 (2018).

9. M. Paven, H. Mayama, T. Sekido, H.-J. Butt, Y. Nakamura, S. Fujii, Light-driven delivery and release of materials using liquid marbles. *Adv. Funct. Mater.* **26**, 3199–3206 (2016).
10. W. Wang, B. Han, Y. Zhang, Q. Li, Y. L. Zhang, D. D. Han, H. B. Sun, Laser-induced graphene tapes as origami and stick-on labels for photothermal manipulation via Marangoni effect. *Adv. Funct. Mater.* **31**, 2006179 (2021).
11. A. Pena-Francesch, J. Giltinan, M. Sitti, Multifunctional and biodegradable self-propelled protein motors. *Nat. Commun.* **10**, 3188 (2019).
12. S. T. Chang, V. N. Paunov, D. N. Petsev, O. D. Velev, Remotely powered self-propelling particles and micropumps based on miniature diodes. *Nat. Mater.* **6**, 235–240 (2007).
13. G. H. Kwon, J. Y. Park, J. Y. Kim, M. L. Frisk, D. J. Beebe, S. H. Lee, Biomimetic soft multifunctional miniature aquabots. *Small* **4**, 2148–2153 (2008).
14. W. Hu, G. Z. Lum, M. Mastrangeli, M. Sitti, Small-scale soft-bodied robot with multimodal locomotion. *Nature* **554**, 81–85 (2018).
15. C. Jin, C. Kruger, C. C. Maass, Chemotaxis and autochemotaxis of self-propelling droplet swimmers. *Proc. Natl. Acad. Sci. U.S.A.* **114**, 5089–5094 (2017).
16. M. I. Kohira, Y. Hayashima, M. Nagayama, S. Nakata, Synchronized self-motion of two camphor boats. *Langmuir* **17**, 7124–7129 (2001).
17. I. Lagzi, S. Soh, P. J. Wesson, K. P. Browne, B. A. Grzybowski, Maze solving by chemotactic droplets. *J. Am. Chem. Soc.* **132**, 1198–1199 (2010).
18. M. Camacho-Lopez, H. Finkelmann, P. Palffy-Muhoray, M. Shelley, Fast liquid-crystal elastomer swims into the dark. *Nat. Mater.* **3**, 307–310 (2004).
19. A. Diguet, R. M. Guillermic, N. Magome, A. Saint-Jalmes, Y. Chen, K. Yoshikawa, D. Baigl, Photomanipulation of a droplet by the chromocapillary effect. *Angew. Chem. Int. Ed.* **48**, 9281–9284 (2009).
20. S. Palagi, A. G. Mark, S. Y. Reigh, K. Melde, T. Qiu, H. Zeng, C. Parmeggiani, D. Martella, A. Sanchez-Castillo, N. Kapernaum, F. Giesselmann, D. S. Wiersma, E. Lauga, P. Fischer, Structured light enables biomimetic swimming and versatile locomotion of photoresponsive soft microrobots. *Nat. Mater.* **15**, 647–653 (2016).
21. Y. Xiao, S. Zarghami, K. Wagner, P. Wagner, K. C. Gordon, L. Florea, D. Diamond, D. L. Officer, Moving droplets in 3D using light. *Adv. Mater.* **30**, 1801821 (2018).
22. Y. Hu, Z. Li, T. Lan, W. Chen, Photoactuators for direct optical-to-mechanical energy conversion: From nanocomponent assembly to macroscopic deformation. *Adv. Mater.* **28**, 10548–10556 (2016).
23. H. Zeng, P. Wasylczyk, D. S. Wiersma, A. Priimagi, Light robots: Bridging the gap between microrobotics and photomechanics in soft materials. *Adv. Mater.* **30**, 1703554 (2018).
24. S. Ma, X. Li, S. Huang, J. Hu, H. Yu, A light-activated polymer composite enables on-demand photocontrolled motion: Transportation at the liquid/air interface. *Angew. Chem. Int. Ed.* **58**, 2655–2659 (2019).
25. Y. Zhao, C. Xuan, X. Qian, Y. Alsaid, M. Hua, L. Jin, X. He, Soft phototactic swimmer based on self-sustained hydrogel oscillator. *Sci. Robot.* **4**, eaax7112 (2019).
26. F. Meng, W. Hao, S. Yu, R. Feng, Y. Liu, F. Yu, P. Tao, W. Shang, J. Wu, C. Song, T. Deng, Vapor-enabled propulsion for plasmonic photothermal motor at the liquid/air interface. *J. Am. Chem. Soc.* **139**, 12362–12365 (2017).
27. H. Sun, M. Liao, J. Li, C. Zhou, J. Deng, X. Fu, S. Xie, B. Zhang, Y. Wu, B. Wang, X. Sun, H. Peng, Programmable actuating systems based on swimming fiber robots. *Carbon* **139**, 241–247 (2018).
28. M. Xiao, C. Jiang, F. Shi, Design of a UV-responsive microactuator on a smart device for light-induced ON-OFF-ON motion. *NPG Asia Mater.* **6**, e128 (2014).
29. M. Liao, H. Sun, X. Tao, X. Xu, Z. Li, X. Fu, S. Xie, L. Ye, Y. Zhang, B. Wang, X. Sun, H. Peng, Alignment of thermally conducting nanotubes making high-performance light-driving motors. *ACS Appl. Mater. Interfaces* **10**, 26765–26771 (2018).
30. D. Okawa, S. J. Pastine, A. Zettl, J. M. J. Frechet, Surface tension mediated conversion of light to work. *J. Am. Chem. Soc.* **131**, 5396–5398 (2009).
31. W. Wang, Y.-Q. Liu, Y. Liu, B. Han, H. Wang, D.-D. Han, J.-N. Wang, Y.-L. Zhang, H.-B. Sun, Direct laser writing of superhydrophobic PDMS elastomers for controllable manipulation via Marangoni effect. *Adv. Funct. Mater.* **27**, 1702946 (2017).
32. S. Rybalko, N. Magome, K. Yoshikawa, Forward and backward laser-guided motion of an oil droplet. *Phys. Rev. E Stat. Nonlin. Soft Matter Phys.* **70**, 046301 (2004).
33. C. Huang, J. A. Lv, X. Tian, Y. Wang, Y. Yu, J. Liu, Miniaturized swimming soft robot with complex movement actuated and controlled by remote light signals. *Sci. Rep.* **5**, 17414 (2015).
34. M. M. Lerch, M. J. Hansen, W. A. Velema, W. Szymanski, B. L. Feringa, Orthogonal photoswitching in a multifunctional molecular system. *Nat. Commun.* **7**, 12054 (2016).
35. S. R. Sershen, G. A. Mensing, M. Ng, N. J. Halas, D. J. Beebe, J. L. West, Independent optical control of microfluidic valves formed from optomechanically responsive nanocomposite hydrogels. *Adv. Mater.* **17**, 1366–1368 (2005).
36. A. Wijaya, S. B. Schaffer, I. G. Pallares, K. Hamad-Schifferli, Selective release of multiple DNA oligonucleotides from gold nanorods. *ACS Nano* **3**, 80–86 (2009).
37. S. Chen, H. Wang, J. Zhou, L. Fang, C. Lu, Z. Xu, Photoresponsive hydrogels with high wavelength selectivity for near-infrared light. *Mater. Lett.* **219**, 163–165 (2018).
38. T. Lan, Y. Hu, G. Wu, X. Tao, W. Chen, Wavelength-selective and rebound-able bimorph photoactuator driven by a dynamic mass transport process. *J. Mater. Chem. C* **3**, 1888–1892 (2015).
39. Y. Liu, B. Shaw, M. D. Dickey, J. Genzer, Sequential self-folding of polymer sheets. *Sci. Adv.* **3**, e1602417 (2017).
40. M. Wang, B. P. Lin, H. Yang, A plant tendril mimic soft actuator with phototunable bending and chiral twisting motion modes. *Nat. Commun.* **7**, 13981 (2016).
41. T. Wang, D. Torres, F. E. Fernandez, C. Wang, N. Sepulveda, Maximizing the performance of photothermal actuators by combining smart materials with supplementary advantages. *Sci. Adv.* **3**, e1602697 (2017).
42. X. Zhang, Z. Yu, C. Wang, D. Zarrouk, J.-W. Seo, J. C. Cheng, A. D. Buchan, K. Takei, Y. Zhao, J. W. Ager, J. Zhang, M. Hettick, M. C. Hersam, A. P. Pisano, R. S. Fearing, A. Javey, Photoactuators and motors based on carbon nanotubes with selective chirality distributions. *Nat. Commun.* **5**, 2983 (2014).
43. Z. Zhu, E. Senses, P. Akcora, S. A. Sukhishvili, Programmable light-controlled shape changes in layered polymer nanocomposites. *ACS Nano* **6**, 3152–3162 (2012).
44. B. Zuo, M. Wang, B. P. Lin, H. Yang, Visible and infrared three-wavelength modulated multi-directional actuators. *Nat. Commun.* **10**, 4539 (2019).
45. A. H. Gelebart, D. J. Mulder, G. Vantomme, A. P. H. J. Schenning, D. J. Broer, A rewritable, reprogrammable, dual light-responsive polymer actuator. *Angew. Chem. Int. Ed. Engl.* **56**, 13436–13439 (2017).
46. M. Gugliotti, M. S. Baptista, M. J. Politi, Laser-induced Marangoni convection in the presence of surfactant monolayers. *Langmuir* **18**, 9792–9798 (2002).
47. H. Kawashima, A. Shioi, R. J. Archer, S. J. Ebbens, Y. Nakamura, S. Fujii, Light-driven locomotion of a centimeter-sized object at the air–water interface: Effect of fluid resistance. *RSC Adv.* **9**, 8333–8339 (2019).
48. X. Zhang, Y. Kong, J. Yan, J. Zhao, Dual-laser-actuated operation of small size objects at a liquid interface. *Appl. Optics* **58**, 5780–5787 (2019).
49. Y. Harada, K. Koyoshi, H. Sakuta, K. Sadakane, T. Kenmotsu, K. Yoshikawa, Emergence of pendular and rotary motions of a centimeter-sized metallic sheet under stationary photoirradiation. *J. Phys. Chem. C* **122**, 2747–2752 (2018).

Acknowledgments

Funding: We acknowledge the financial support from the MOST of China (nos. 2016YFA0200800 and 2019YFA0709200). **Author contributions:** Conceptualization: Y.L. and K.H. Methodology: K.H., Y.L., and D.G. Investigation: K.H., H.L., D.G., and Y.S. Visualization: K.H. Supervision: K.S. Writing—original draft: K.H. Writing—review and editing: K.H., Y.L., K.S., and D.G. **Competing interests:** The authors declare that they have no competing interests. **Data and materials availability:** All data needed to evaluate the conclusions in the paper are present in the paper and/or the Supplementary Materials.

Submitted 1 March 2021
Accepted 22 July 2021
Published 10 September 2021
10.1126/sciadv.abh3051

Citation: K. Hou, D. Guan, H. Li, Y. Sun, Y. Long, K. Song, Programmable light-driven swimming actuators via wavelength signal switching. *Sci. Adv.* **7**, eabh3051 (2021).

ScienceAdvances

Programmable light-driven swimming actuators via wavelength signal switching

Kai HouDongshi GuanHangyu LiYongqi SunYue LongKai Song

Sci. Adv., 7 (37), eabh3051. • DOI: 10.1126/sciadv.abh3051

Science Advances (ISSN) is published by the American Association for the Advancement of Science. 1200 New York Avenue NW, Washington, DC 20005. The title *Science Advances* is a registered trademark of AAAS.